

Long-wave Dynamics of an Inextensible Planar Membrane in an Electric Field

Y.-N. Young¹, Shравan Veerapaneni² and Michael J. Miksis³

¹Department of Mathematical Sciences
and Center for Applied Mathematics and Statistics,

New Jersey Institute of Technology, Newark, New Jersey 07102 USA

²Department of Mathematics, University of Michigan, Ann Arbor, Michigan 48109, USA

³Department of Engineering Sciences and Applied Mathematics, Northwestern University,
Evanston, Illinois 60208, USA

(Received 11 November 2013)

We investigate the long-wave nonlinear dynamics of an inextensible capacitive elastic membrane under electric fields. In the lubrication framework we derive a nonlinear equation for the membrane height with an integral constraint. Linear analysis on the tensionless membrane in a dc field gives the linear growth rate in terms of membrane conductance and electric properties in the bulk. The long-wave formulation allows us to analytically derive the equilibrium membrane profile in a dc field. Numerical simulations of an inextensible membrane under ac fields elucidate how variation of the membrane tension correlates to the non-linear membrane dynamics. Different membrane dynamics, such as undulation and flip-flop, is found at different electric field strength and membrane area. In particular a traveling wave on the membrane is found as a response to a periodic ac field in the perpendicular direction.

1. Introduction

The cellular membrane, comprising mainly of two lipid leaflets, is essential to a wide range of cellular functions partly because the membrane regulates the transport of particles (such as ions and macromolecules) between interior and exterior cellular space. In engineering applications both weak (Antov *et al.* 2005) and strong electric fields are used to induce macro pores in the cell membrane for drug and DNA delivery into living cells (see Sadik *et al.* (2011) and references therein). External direct current (dc) and/or alternating current (ac) electric fields have also been used to destabilize planar lipid membranes to facilitate the formation of vesicles (liposomes, self-enclosing unilamellar membranes) in electroformation (Angelova & Dimitrov 1986), where the interplay between external electric fields and the membrane forces (such as membrane tension and bending forces) underlies the membrane instability. Experimental studies revealed how a stack of lipid bilayer membranes unbind from the substrate under electric fields (Constantin *et al.* 2005), and how a free-floating membrane can become unstable under an ac field below 100 Hz (Lecuyer *et al.* 2006).

Theoretical studies on membrane destabilization due to electric fields show that both membrane thickness fluctuations (Weaver & Chizmadzhev 1996) and bending modes (Sens & Isambert 2002; Lacoste *et al.* 2007; Schwalbe *et al.* 2011) can destabilize the planar membrane. Membrane conductance and mismatch in dielectric fluid properties are also essential to the linear instability of a planar lipid bilayer membrane in both dc (Seiwert *et al.* 2012) and ac (Seiwert & Vlahovska 2013) electric fields. Negative membrane tension and the ion currents in the diffuse layers near the membrane give

rise to undulations of an unsupported planar membrane under electric fields. The planar membrane become linearly unstable and the undulation can be amplified once the electric field is above a threshold at which the negative tension exceeds the initial tension in the membrane (Sens & Isambert 2002). The other source of instability caused by the ion currents near the membrane (Lacoste *et al.* 2007, 2009; Ziebert *et al.* 2010; Ziebert & Lacoste 2010, 2011) gives rise a relaxation rate proportional to wavenumber squared. For giant vesicles subjected to an electric field, the electric pulse duration and the subsequent relaxation process are found to be essential to membrane deformation and poration (Riske & Dimova 2005; Bezlyepkina *et al.* 2009; Zhang *et al.* 2013; McConnell *et al.* 2013).

Long wavelength formulation of the electrohydrodynamics of an interface between two leaky dielectric fluids under dc or ac (see Roberts & Kumar 2009, 2010) fields have uncovered both the linear instability and weakly nonlinear dynamics related to pillar formation that are consistent with experiments (Schaffer *et al.* 2000; Pease & Russel 2002; Thaokar & Kumaran 2005; Wu & Russel 2009). The lubrication theory has also been successfully applied to understand the elasto-hydrodynamics of a elastic sheet lubricated by a thin layer of fluid (Hosoi & Mahadevan 2004). In that analysis the bending force is dominant over the tension, and the elastic sheet area may vary due to the dynamics. The balance between bending force and the van der Waals forces was found essential to the observed bursting in the elastic sheet with a constant flux in the lubricating layer. More recently Blount *et al.* (2012) developed a lubrication model to study flow beneath a semipermeable inextensible membrane and obtained equilibrium solutions and bifurcation structure as a function of drying parameters. In this work, we apply the long wavelength analysis to two layers of leaky dielectric fluid separated by an elastic inextensible membrane which is a sharp-interface model for the lipid bilayer membrane.

The main components of the sharp-interface approximation of the lipid bilayer membrane are its elastic properties, inextensibility, capacitance and conductance. The lipid bilayer membrane is inextensible because both the area per lipid and the total lipid number are conserved in each leaflet. In this work we use membrane forces derived from the Helfrich membrane energy $\mathcal{F} = \int_{\Omega} \left(\frac{K}{2} \kappa^2 + \Sigma \right) \partial\Omega$, where Ω is the membrane surface, K is the bending modulus, and κ is the curvature. The membrane tension Σ is a Lagrange multiplier to be determined from the constant surface area constraint (Seifert 1995). The inextensible elastic membrane also acts as a (leaky) capacitor where the trans-membrane potential varies due to the currents on and across the two leaflets. In biological cells the trans-membrane currents may be due to pores and ion channels. The currents on the membrane are the ohmic currents from the bulk to the membrane in the leaky dielectric model.

Without membrane conductance it is found that asymmetry in fluid conductivities gives rise to a transient instability in a dc electric field (Schwalbe *et al.* 2011). With membrane conductance, the capacitive membrane can be linearly unstable (Seiwert *et al.* 2012). In an ac electric field a purely capacitive membrane can be rendered unstable at low field frequencies, while at high frequencies even a conducting membrane can become stable (Seiwert & Vlahovska 2013). The main goal of this work is to investigate the dynamics of a conducting capacitive membrane in the long wavelength formulation that would allow us to examine the membrane stability beyond the linear stability for a flat membrane.

This paper is organized as follows: The problem description is given in § 2, followed by § 2.1 where we formulate the long-wave dynamics of an elastic, inextensible membrane separating two leaky dielectric fluids. The equilibrium profile for a non-conducting membrane in a dc field is derived in § 2.2, and the linear stability for a flat tension membrane in a dc field is analyzed in In § 2.3. The numerical implementation of a semi-implicit

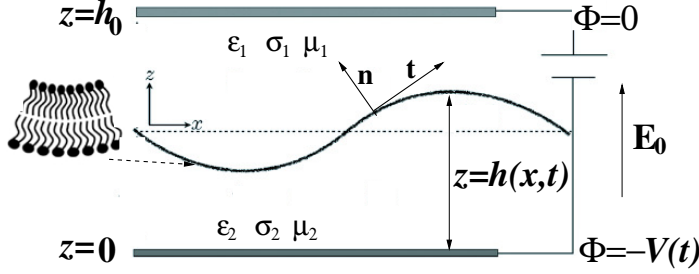


FIGURE 1. A planar lipid bilayer membrane (at $z = h(x, t)$) separates two leaky dielectric fluids. The electric potential Φ is fixed on the top ($\Phi = 0$) and bottom ($\Phi = -V(t)$) walls. \mathbf{n} is the outward unit normal on the membrane, and \mathbf{t} is the unit tangent.

scheme for solving the governing long-wave equations is given in § 2.4. In a dc field the displacement current is negligible and our numerical simulations show that the membrane dynamics (with or without membrane conductance) is always towards the steady equilibrium that is similar to those described in § 2.2. Therefore in § 3 we focus on the dynamics of a conducting membrane in an ac field. We first examine the linear stability of a tensionless flat membrane in an ac field in § 3.1. In the rest of § 3 we study how the membrane instability and its non-linear dynamics depend on the membrane tension and the correlation with induced surface charge distribution. In § 3.4 we present a novel “alternating wave” with large membrane excess length under strong ac fields. We summarize our findings and provide a discussion on the implications of the results in § 4.

2. Problem formulation

We consider two layers of leaky dielectric fluid under an imposed electric field $E_0 \hat{z}$. The two fluids are separated by an inextensible elastic planar membrane (at $z = h(x, t)$) formed by a charge-free lipid bilayer with dielectric constant ε_m and conductivity σ_m . The bilayer thickness $d \sim 5$ nm, which is small enough for us to treat the membrane as a two-dimensional interface with effective capacitance $C_m = \varepsilon_m/d$ and conductance $G_m = \sigma_m/d$. Each layer of fluid is specified by its permittivity (ε), conductivity (σ) and viscosity (μ), with the subscripts in figure 1 denoting either top (‘1’) or bottom (‘2’) fluid layer. The electric field is irrotational, $\mathbf{E}_j = -\nabla\Phi_j$, and the electric potential Φ satisfies the Laplace equation

$$\nabla^2 \Phi_j = 0 \quad j = 1, 2, \quad (2.1)$$

because the bulk fluids become electro-neutral over a charging time $t_{c,j} = \varepsilon_j/\sigma_j \ll 1$. Within each layer the two-dimensional fluid velocity $\mathbf{u}_j = (u_j, w_j)$ satisfies the incompressible Navier-Stokes equations

$$\rho_j \left(\frac{\partial \mathbf{u}_j}{\partial t} + \mathbf{u}_j \cdot \nabla \mathbf{u}_j \right) = -\nabla p_j + \mu_j \nabla^2 \mathbf{u}_j, \quad (2.2)$$

$$\nabla \cdot \mathbf{u}_j = 0, \quad (2.3)$$

where $j = 1$ or $j = 2$ for the top or bottom fluid. p_j is pressure, and ρ_j is the fluid density which we assume to be the same for both layers.

In the leaky dielectric model the induced charge of the diffuse layers around the membrane is effectively described as the surface charge density $q_1 = \mathbf{n} \cdot \varepsilon_1 \mathbf{E}_1 - C_m V_m$ at $z = h^+$ (the membrane interface in contact with fluid 1) $q_2 = C_m V_m - \mathbf{n} \cdot \varepsilon_2 \mathbf{E}_2$ at $z = h^-$ (the membrane interface in contact with fluid 2), and $q = q_1 + q_2 = \mathbf{n} \cdot (\varepsilon_1 \mathbf{E}_1 - \varepsilon_2 \mathbf{E}_2)$

at $z = h$. In this work we adopt the formulation in Seiwert *et al.* (2012), and focus on the limit of fast bulk charge relaxation. From the conservation of currents across the membrane

$$\mathbf{n} \cdot \left(\sigma_2 \mathbf{E}_2 + \varepsilon_2 \frac{\partial \mathbf{E}_2}{\partial t} \right) + \nabla_s \cdot (\varepsilon_2 \mathbf{u} E_{2n}) = \mathbf{n} \cdot \left(\sigma_1 \mathbf{E}_1 + \varepsilon_1 \frac{\partial \mathbf{E}_1}{\partial t} \right) + \nabla_s \cdot (\varepsilon_1 \mathbf{u} E_{1n}), \quad (2.4)$$

at $z = h$ with $E_{in} = \mathbf{n} \cdot \mathbf{E}_i$ and $\nabla_s = (\mathbf{I} - \mathbf{nn})\nabla$ the surface gradient. The electric potential is discontinuous across the biomimetic membrane and the transmembrane potential $V_m \equiv \Phi_1(z = h^+) - \Phi_2(z = h^-)$ is given by

$$\mathbf{n} \cdot \left(\sigma_i \mathbf{E}_i + \varepsilon_i \frac{\partial \mathbf{E}_i}{\partial t} \right) + \nabla_s \cdot (\varepsilon_i \mathbf{u} E_{in}) = C_m \frac{\partial V_m}{\partial t} + \nabla_s \cdot (\mathbf{u} C_m V_m) + G_m V_m. \quad (2.5)$$

The membrane capacitance $C_m \approx 0.01 \text{ F/m}^2$ and the membrane conductance $G_m \approx 10^{-3} - 10^6 \text{ S/m}^2$.

2.1. Long-wave formulation

In the long-wave formulation, the aspect ratio of the height (h_0) to the characteristic horizontal length (l) is assumed to be small ($\epsilon = h_0/l \ll 1$). Similar to the scaling in Hosoi & Mahadevan (2004), we non-dimensionalize equations 2.1, 2.2, 2.3, and 2.5 by the characteristic length and velocity ($\frac{h_0}{\epsilon}, h_0$) and $(U_0, \epsilon U_0)$ in the (x, z) directions, respectively. The pressure is scaled by $\frac{\mu_2 U_0}{\epsilon h_0}$, time by $\frac{h_0}{\epsilon U_0}$, and the electric potential by $E_0 h_0$. The dimensionless variables (with bars) are

$$\bar{z} = \frac{z}{h_0}, \quad \bar{x} = \frac{x}{h_0/\epsilon}, \quad \bar{u} = \frac{u}{U_0}, \quad \bar{w} = \frac{w}{\epsilon U_0}, \quad \bar{p} = \frac{p}{\mu_2 U_0 / \epsilon h_0}, \quad \bar{t} = \frac{t}{h_0 / \epsilon U_0}, \quad \text{and} \quad \bar{V}_m = \frac{V_m}{E_0 h_0}.$$

The dimensionless equations are (after dropping bars)

$$\epsilon Re_i (\partial_t u_i + u_i \partial_x u_i + w_i \partial_z u_i) = -\frac{\mu_2}{\mu_i} \partial_x p_i + \partial_z^2 u_i + \epsilon^2 \partial_x^2 u_i, \quad (2.6)$$

$$\epsilon^3 Re_i (\partial_t w_i + u_i \partial_x w_i + w_i \partial_z w_i) = -\frac{\mu_2}{\mu_i} \partial_z p_i + \epsilon^2 (\partial_z^2 w_i + \epsilon^2 \partial_x^2 w_i), \quad (2.7)$$

$$\partial_x u_i + \partial_z w_i = 0, \quad (2.8)$$

$$\nabla^2 \Phi_i = \partial_{xx}^2 \Phi_i + \epsilon^2 \partial_{zz}^2 \Phi_i = 0, \quad (2.9)$$

$$c_m \left(\frac{\partial V_m}{\partial t} + u \frac{\partial V_m}{\partial x} \right) + g_m V_m = E_{1n} + \alpha \left(\frac{\partial E_{1n}}{\partial t} + u \frac{\partial E_{1n}}{\partial x} \right). \quad (2.10)$$

The dimensionless parameters are

$$Re_i \equiv \frac{U_0 h_0}{\mu_i / \rho_i}, \quad \alpha = \frac{\varepsilon_1 U_0}{h_0 \sigma_1} \epsilon, \quad c_m = \frac{C_m U_0}{\sigma_1} \epsilon, \quad \text{and} \quad g_m = \frac{G_m h_0}{\sigma_1}.$$

There are several time scales involved in this system: The capacitive membrane charges on a time scale (Seiwert & Vlahovska 2013) $t_m = \frac{h_0 C_m}{\sigma_1} \frac{1 + \sigma_r}{1 + g_m (1 + \sigma_r)}$, the balance between viscous stress and the electric shear traction gives $t_{EHD,j} = \frac{\mu_j}{\varepsilon_j E_0^2}$, while bending resistance to changes in membrane curvature gives another time scale $t_{K,j} = \frac{\mu_j}{K q^3}$ for a membrane undulation with wave number q . Typical values for the conductivity $\sigma \approx 10^{-6} - 10^{-3} \text{ S/m}$, $\varepsilon \approx 10^{-10} \text{ F/m}$, $K \approx 10^{-19} \text{ J}$, $h_0 \approx 10 - 100 \text{ } \mu\text{m}$, $\mu \approx 10^{-3} \text{ Pa s}$, $E_0 \approx 1 \text{ kV/m}$. We choose $U_0 = \frac{\sigma_1}{C_m \epsilon}$ such that $c_m = 1$, and typically $U_0 \approx \mathcal{O}(1)$ due to the small conductivity and large membrane capacitance.

At the bottom wall, we have $u_2(0) = w_2(0) = 0$ and $\Phi_2(0) = -\nu(t)$ while at the

top wall $u_1(1) = w_1(1) = 0$ and $\Phi_1(1) = 0$. On the elastic membrane $z = h(x, t)$, the kinematic continuity condition gives

$$w_1(x, h(x, t)) = w_2(x, h(x, t)) = \partial_t h + u_1|_{z=h} \partial_x h = \partial_t h + u_2|_{z=h} \partial_x h. \quad (2.11)$$

The stress balance on the elastic membrane gives

$$(-p_1 + p_2) \mathbf{n} + [[\mathbf{T}^{hd} + \mathbf{T}^{el}]] \cdot \mathbf{n} = \mathbf{f}^m, \quad (2.12)$$

where $[[\cdot]]$ denotes the difference between top and bottom layers. $(\mathbf{T}^{hd})_{ij} \equiv \mu (\partial_i v_j + \partial_j v_i)$ is the ij -th component of the viscous stress tensor, and $(\mathbf{T}^{el})_{ij} \equiv \varepsilon (\mathbf{E}_i \mathbf{E}_j - \frac{1}{2} \mathbf{E}^2 \delta_{ij})$ is the ij -th component of the Maxwell electric stress. For membrane force \mathbf{f}^m we ignore the high-order curvature term and the Gaussian curvature term due to the long-wave planar geometry and write $\mathbf{f}^m = -(-2K \nabla_s^2 \kappa + 2\Sigma \kappa) \mathbf{n} + \nabla_s \Sigma$, with K the membrane bending rigidity, κ the membrane mean curvature, and Σ the membrane surface tension to be determined from the membrane incompressibility condition.

Following the procedures in the long-wave analysis for a porous inextensible elastic membrane (Blount *et al.* 2012), we expand the dependent variables (u, w, p) in ε and (Φ, Σ) in ε^2 . We find that, at the leading order the membrane outward normal $\mathbf{n} = \frac{(-\varepsilon \partial_x h, 1)}{\sqrt{1 + \varepsilon^2 \partial_x h^2}} \sim (-\varepsilon \partial_x h, 1)$, the membrane tangent $\mathbf{t} = \frac{(1, \varepsilon \partial_x h)}{\sqrt{1 + \varepsilon^2 \partial_x h^2}} \sim (1, \varepsilon \partial_x h)$, and the membrane curvature $\kappa = \frac{\varepsilon^2 h_{xx}}{(1 + \varepsilon^2 \partial_x h^2)^{3/2}} \sim \varepsilon^2 h_{xx}$. The leading order electric potential in the bulk is: $\Phi_1 = A(x, t)(z - 1)$ and $\Phi_2 = C(x, t)z - \nu(t)$ with $\nu(t) = V(t)/V_0$.

The leading order normal stress balance gives a relation between p_1 and p_2 , and the leading order tangential stress balance gives a relation between the Marangoni stress and the viscous shear stress. The leading order horizontal velocity field can be written as $u_i = \frac{\mu_2}{\mu_i} \frac{\partial_x p_i}{2} z^2 + a_i z + b_i$, where a_i and b_i are to be determined by the velocity boundary conditions (Oron *et al.* 1997):

$$a_1 + b_1 = -\frac{1}{2\mu_r} (p_2 + g + \beta_1)_x \equiv D', \quad (2.13)$$

$$ha_1 + b_1 - ha_2 = \frac{h^2}{2} \left[p_2 \left(1 - \frac{1}{\mu_r} \right) - \frac{g + \beta_1}{\mu_r} \right]_x \equiv E', \quad (2.14)$$

$$\mu_r a_1 - a_2 = h(-g - \beta_1)_x - \frac{\bar{C}}{2} \partial_x \Sigma_1 - \beta_2 \equiv F', \quad (2.15)$$

with $\beta_2 \equiv \beta [\varepsilon_r (AA_x(h - 1) - A^2 h_x) - (Cxh - Ch_x)C]$, $g \equiv \bar{C} \Sigma_0 \partial_x^2 h - \bar{K} \partial_x^4 h$, and $\beta_1 \equiv \frac{\beta}{2} (\varepsilon_r A^2 - C^2)$. The dimensionless parameters in the above equations are defined as

$$\beta \equiv \frac{\varepsilon_2 E_0^2 h_0 \varepsilon}{\mu_2 U_0} = \frac{\varepsilon_2 E_0^2 h_0 C_m \varepsilon^2}{\mu_2 \sigma_1}, \quad \bar{K} \equiv \frac{2K \varepsilon^5}{\mu_2 U_0 h_0^2} = \frac{2KC_m \varepsilon^6}{\mu_2 \sigma_1 h_0^2}, \quad \bar{C} \equiv \frac{2\gamma_0 \varepsilon^3}{\mu_2 U_0} = \frac{2\gamma_0 C_m \varepsilon^4}{\mu_2 \sigma_1}, \quad (2.16)$$

where γ_0 is a scaling factor for membrane tension, the viscosity ratio $\mu_r = \mu_1/\mu_2$, conductivity ratio $\sigma_r = \sigma_1/\sigma_2$, and permittivity ratio $\varepsilon_r = \varepsilon_1/\varepsilon_2$. The solution (a_1, b_1, a_2) is computed as

$$a_1 = \frac{D' - E' + F'h}{1 - h + \mu_r h}, \quad (2.17)$$

$$b_1 = D' - \frac{D' - E' + F'h}{1 - h + \mu_r h}, \quad (2.18)$$

$$a_2 = \frac{\mu_r (D' - E') - F'(1 - h)}{1 - h + \mu_r h}. \quad (2.19)$$

The membrane tension $\Sigma \approx \Sigma_0 + \epsilon^2 \Sigma_1$ remains to be determined from the inextensibility (constant surface area) of the lipid membrane, which can be recast in terms of the incompressibility condition for the velocity on the membrane

$$\nabla_s \cdot \vec{v} = \epsilon (\partial_x u + h_x \partial_z u) + \epsilon^3 (-(\partial_x h)^2 \partial_x u + \partial_x h \partial_x w) + \mathcal{O}(\epsilon^5) = 0. \quad (2.20)$$

At leading order the surface incompressibility gives

$$[\partial_x u + h_x \partial_z u]_{z=h} = \frac{d}{dx} u(x, z = h(x, t)) = 0, \quad (2.21)$$

which is the condition for the local membrane area conservation. In addition, the total surface area \mathcal{L}

$$\mathcal{L} \equiv \int_{-L/2}^{L/2} \sqrt{1 + \epsilon^2 h_x^2} dx \sim L + \frac{\epsilon^2}{2} \int_{-L/2}^{L/2} h_x^2 dx + \mathcal{O}(\epsilon^4).$$

Consequently, a constant excess area $\mathcal{L} - L$ at $\mathcal{O}(\epsilon^2)$ implies a globally conserved surface area at $\mathcal{O}(\epsilon^2)$

$$\mathcal{L} - L = \frac{\epsilon^2}{2} \int_{-L/2}^{L/2} h_x^2 dx = \text{constant}. \quad (2.22)$$

The constant excess area constraint determines the homogeneous membrane tension Σ_0 , while the local area conservation (equation 2.21) gives the gradient of the spatially inhomogeneous tension Σ_{1x} in terms of h and p_{2x} :

$$\Sigma_{1x} = \frac{1}{\bar{C}} [-(1-h)(g_x + \beta_{1x}) - p_{2x} + 2\beta_2] - \frac{2c_1(1 + (-1 + \mu_r)h)}{\bar{C}(1-h)h}, \quad (2.23)$$

where the constant $c_1 \equiv u(x, z = h(x, t))$ is from integrating equation 2.21. Consequently, the gradient of pressure p_2 can be expressed as

$$p_{2x} = \frac{(-1+h)^3(g_x + \beta_{1x}) + f_1}{(1-h)^3 + \mu_r h^3}, \quad (2.24)$$

where f_1 is a second integration constant obtained from integrating the equation that involves p_{2xx} . Putting everything together in equation 2.11, we obtain the evolution equation for h as

$$\partial_t h + \partial_x \left[-\frac{(-1+h)^3 h^3 (g_x + \beta_{1x}) + f_1 h^3}{12((1-h)^3 + \mu_r h^3)} + \frac{c_1 h}{2} \right] = 0. \quad (2.25)$$

In three dimensions, the evolution equation for $h(x, y, t)$ is

$$\partial_t h + \nabla \left[-\frac{(-1+h)^3 h^3 \nabla(G + \beta_1) + \vec{f} h^3}{12((1-h)^3 + \mu_r h^3)} + \frac{\vec{c} h}{2} \right] = 0, \quad (2.26)$$

with $\vec{f} = (f_1, f_2)$, $\vec{c} = (c_1, c_2)$, $G \equiv \bar{C} \Sigma_0 \nabla^2 h - \bar{K} \nabla^4 h$ and $\nabla \equiv (\partial_x, \partial_y)$. In the following we set the integration constants \vec{f} and \vec{c} zero.

The electric field strength A and C satisfy

$$A + \alpha \frac{dA}{dt} = \frac{1}{\sigma_r} C + \frac{\alpha}{\epsilon_r} \frac{dC}{dt}, \quad (2.27)$$

where $\frac{d}{dt} = \frac{\partial}{\partial t} + u \partial_x$. The transmembrane potential $V_m \equiv \Phi_1 - \Phi_2|_{z=h} = A(h-1) - Ch + \nu$ satisfies the following (dimensionless) equation at leading order

$$c_m \frac{dV_m}{dt} + g_m V_m = A + \alpha \frac{dA}{dt}. \quad (2.28)$$

At the leading order the convection terms vanish because we set the integration constant $u(z = h(x, t)) = c = 0$ in the derivation. As a result $d/dt = \partial/\partial t$ in equations 2.27-2.28. This is consistent with the assumption of vanishing charge convection on the membrane in the linear analyses for a flat tensionless membrane (Seiwert *et al.* 2012; Seiwert & Vlahovska 2013). Furthermore, the convection of the induced surface charge has been shown to have little effect on the electro-deformation of a viscous drop (Feng & Beard 1991).

Equations 2.25 and 2.28, together with the integral constraint in equation 2.22, are the governing long-wave equations for an inextensible elastic membrane under an electric field. Six boundary conditions are needed to complete the problem formulation. In § 3 we will focus on periodic boundary conditions. For our governing long wave equation, the periodic boundary conditions are closely related to the boundary conditions: $h_x = h_{xxx} = (g + \beta_1)_x = 0$ at $x = \pm L/2$ associated with multiple blisters for a thin film (Blount *et al.* 2012). For both the periodic and the multiple blister boundary conditions, the homogeneous membrane tension Σ_0 can be explicitly expressed in terms of h by taking the derivative of equation 2.22 with respect to time and performing integration by parts:

$$\Sigma_0 = \frac{\int_{-L/2}^{L/2} F h_{xxx} \left[\bar{K} h_{xxxx} - \frac{\beta}{2} (\varepsilon_r A^2 - C^2)_x \right] dx}{\bar{C} \int_{-L/2}^{L/2} F h_{xxx}^2 dx}, \quad (2.29)$$

where the function F is defined as

$$F = -\frac{(-1 + h)^3 h^3}{12 [(1 - h)^3 + \mu_r h^3]}. \quad (2.30)$$

For a dc electric field, the displacement current $\frac{dA}{dt}$ (associated with charge relaxation on the surface) is small and often neglected because $\alpha \ll 1$. Setting $\alpha = 0$ in equation 2.27 gives $C = \sigma_r A$, and equation 2.28 can be integrated to give

$$V_m = V_m(0) + \frac{1}{c_m \chi(t)} \int_0^t -\frac{\chi(t')}{(1 - \sigma_r)h - 1} dt', \quad (2.31)$$

$$\chi(t) = e^{\frac{g_m t}{c_m} - \frac{1}{c_m} \int_0^t \frac{1}{(1 - \sigma_r)h - 1} dt'}. \quad (2.32)$$

In the absence of membrane conductance ($g_m = 0$), the above equation can be easily recast to give

$$E(x, t) = E(x, 0) \frac{-1 + (1 - \sigma_r)h(x, 0)}{-1 + (1 - \sigma_r)h(x, t)} e^{I(t)}, \quad (2.33)$$

with

$$I(t) = \frac{1}{c_m} \int_0^t \frac{1}{-1 + (1 - \sigma_r)h(t')} dt'. \quad (2.34)$$

It can be easily seen that $I(t) < 0$ as long as $\sigma_r \geq 0$ and $0 < h < 1$. Therefore the electric field $E \rightarrow 0$ as the non-conducting capacitive membrane charges over time.

2.2. Equilibrium Profile for a Non-conducting Membrane ($g_m = 0$) in dc Fields

For a non-conducting membrane ($g_m = 0$) in a dc electric field ($\alpha = 0$), the following simple equilibrium analysis gives admissible equilibrium profiles determined by the volume (area) under the membrane and the total area (length) of the two-dimensional (one-dimensional) membrane. No such simple equilibrium results are available for a conducting membrane ($g_m > 0$) or in an ac electric field (ν is a function of time).

For a non-conducting ($g_m = 0$) capacitive membrane in a dc field, the electric fields A and C decays exponentially to zero as the membrane charges up. At equilibrium the profile satisfies the simple equation

$$\frac{d}{dx} \left[F \frac{dg}{dx} \right] = 0 \quad (2.35)$$

for $x \in (-L/2, L/2)$ with either (1) periodic boundary conditions, or (2) $h_x = h_{xxx} = g_x = 0$ at $x = \pm L/2$. The function F (equation 2.30) is non-zero as long as $0 < h < 1$. In addition the leading-order excess length of the interface and area (or volume in three dimensions) under the interface must remain constant:

$$\int_{-L/2}^{L/2} (h_x)^2 dx \equiv S = \text{constant}, \quad \int_{-L/2}^{L/2} h dx \equiv \theta = \text{constant}. \quad (2.36)$$

Integrating equation 2.35 once and setting the integration constant to zero, we obtain

$$\frac{d}{dx} \left[\bar{C} \Sigma_0 \frac{d^2 h}{dx^2} - \bar{K} \frac{d^4 h}{dx^4} \right] = 0. \quad (2.37)$$

For periodic boundary conditions, the equilibrium profile takes the form

$$h = a \cos \left(\frac{2n\pi x}{L} \right) + b \sin \left(\frac{2n\pi x}{L} \right) + \frac{\theta}{L}, \quad (2.38)$$

where integer n and membrane tension Σ_0 are related via $n^2 = -\frac{\bar{C}\Sigma_0}{\bar{K}} \left(\frac{L}{2\pi} \right)^2$ and $\Sigma_0 < 0$. a and b are related to S via $\left(\frac{2n\pi}{L} \right)^2 \frac{(a^2+b^2)L}{2} = S$. For $h_x = h_{xxx} = g_x = 0$ at $x = \pm L/2$, the equilibrium profile in equation 2.38 splits into a symmetric profile

$$h(x) = \pm \frac{\sqrt{2S/L}}{2N\pi/L} \cos \left(\frac{2N\pi x}{L} \right) + \frac{\theta}{L}, \quad (2.39)$$

and an anti-symmetric profile

$$h(x) = \pm \frac{\sqrt{2S/L}}{2N\pi/L} \sin \left(\frac{2N\pi x}{L} \right) + \frac{\theta}{L} \quad (2.40)$$

with $N^2 = -\frac{\bar{C}\Sigma_0}{\bar{K}} \left(\frac{L}{2\pi} \right)^2$. N is an integer for the symmetric profiles, and a half-integer for the anti-symmetric profile.

For a given membrane excess length S and an area θ under the membrane in two dimensions, m has to satisfy the following inequalities (from $0 < h < 1$)

$$0 < -\frac{\sqrt{2S/L}}{2m\pi/L} + \frac{\theta}{L}, \quad \frac{\sqrt{2S/L}}{2m\pi/L} + \frac{\theta}{L} < 1, \quad (2.41)$$

with $m = n$ for the periodic boundary conditions and $m = N$ for the blistering boundary conditions. The corresponding total energy of the membrane interface is computed as

$$E = \bar{K} \int_{-L}^L (h_{xx})^2 dx + \Sigma_0 \bar{C} S = - \left(\frac{2m\pi}{L} \right)^2 \bar{K} S. \quad (2.42)$$

The most stable equilibrium will be given by one of the plausible values of m that minimizes the membrane energy in equation 2.42. For a capacitive membrane with conductance, no such simple expression for the equilibrium profile was found because of the nonlinearity from the non-vanishing E at equilibrium. Figure 2(a) illustrates the variation of m with S for $\theta/L = 1/2$.

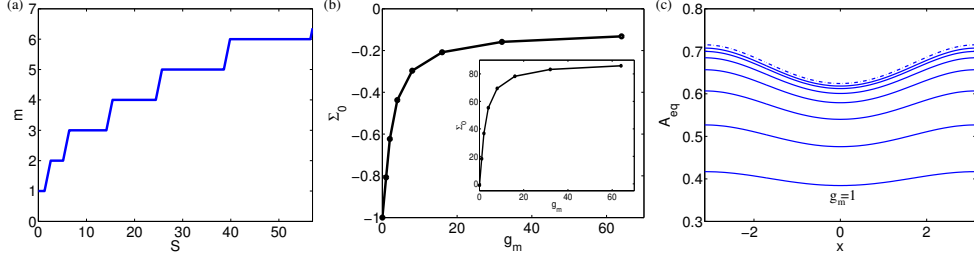


FIGURE 2. (a) Equilibrium mode number as a function of excess length S for $\theta/L = 1/2$. (b) Equilibrium membrane tension as a function of membrane conductance from simulations with parameters. (c) Equilibrium electric field profile A_{eq} as the membrane conductance increases (with a multiple of 2) from bottom ($g_m = 1$) to top ($g_m = \infty$ for the dashed line).

2.3. Linear Stability of a Tensionless Flat Membrane in a dc Field

Linear stability analysis on a flat capacitive conducting tension-free membrane has been conducted for both dc (Seiwert *et al.* 2012) and ac (Seiwert & Vlahovska 2013) fields. In contrast to the stability of a fluid interface that depends solely on the mismatch of the fluid dielectric properties (see Craster & Matar 2005; Roberts & Kumar 2009), the membrane conductance is found to be essential for the linear instability (Seiwert *et al.* 2012), while the linear growth rate is reduced by the electric field frequency in the ac field (Seiwert & Vlahovska 2013).

In the long-wave formulation the membrane tension responds to the bending and electric forces (equation 2.29) to keep the membrane inextensible. We will linearize the long-wave equations around the base state

$$h_0 = \text{constant}, \quad A_0 = \frac{g_m}{1 + g_m[\sigma_r h_0 + (1 - h_0)]}, \quad C_0 = \sigma_r A_0. \quad (2.43)$$

The shape fluctuations can be written as $h(x, t) = h_0 + \delta h e^{iQx + \lambda t}$ (with Q the wave number and λ the growth rate) with similar expressions for A and C . Focusing on the dc field ($\alpha = 0$ and $\nu = 1$) case, these fluctuations can be substituted into the long-wave model (equations 2.25, 2.27 and 2.28) and then linearized. For a tensionless membrane, an analytical form for the growth rate can be found in the limit $Q \rightarrow 0$:

$$\lambda \approx \frac{\beta(\varepsilon_r - \sigma_r^2)(1 - \sigma_r)g_m^3}{96(1 + \mu_r)[1 + (\sigma_r + 1)g_m/2]^3} Q^2 - \frac{\bar{K}}{96(1 + \mu_r)} Q^6, \quad (2.44)$$

with $h_0 = 1/2$. Equation 2.44 shows that the flat tension-less membrane can be unstable when $(\varepsilon_r - \sigma_r^2)(1 - \sigma_r)g_m > 0$ (assuming that the membrane conductance $g_m \geq 0$), consistent with the conclusion in Seiwert *et al.* (2012). However, the dependence of the growth rate on Q is quadratic from our long-wave formulation, while a cubic dependence is reported in Seiwert *et al.* (2012) for a membrane in free space. From equation 2.44 the maximum growth rate (λ_{max}) and the corresponding wavenumber Q_{max} can be computed as

$$Q_{max} = \sqrt[4]{\frac{\beta(\varepsilon_r - \sigma_r^2)(1 - \sigma_r)}{\bar{K}} \left(\frac{g_m}{(1 + \frac{\sigma_r + 1}{2}g_m)} \right)^3} \sim \bar{K}^{-1/4}, \quad (2.45)$$

$$\lambda_{max} = \frac{\beta(\varepsilon_r - \sigma_r^2)(1 - \sigma_r)g_m^3}{144(1 + \mu_r)[1 + (\sigma_r + 1)g_m/2]^3} Q_{max}^2 \sim \bar{K}^{-1/2}. \quad (2.46)$$

In the limit of large membrane conductance $g_m \rightarrow \infty$,

$$Q_{max} \rightarrow \sqrt[4]{\frac{8\beta(\varepsilon_r - \sigma_r^2)(1 - \sigma_r)}{\bar{K}(\sigma_r + 1)^3}}, \quad \lambda_{max} \rightarrow \frac{\beta(\varepsilon_r - \sigma_r^2)(1 - \sigma_r)}{18(1 + \mu_r)(\sigma_r + 1)^3} Q_{max}^2. \quad (2.47)$$

2.4. Numerical Implementation

The evolution equation for the membrane height (equation 2.25) is a sixth-order nonlinear differential equation. As a result, an explicit time-marching scheme has stringent stability constraint and will be impractical to simulate the physics even in the one-dimensional case. To overcome the restriction on time-step, we formulate a semi-implicit scheme similar to that of Veerapaneni *et al.* (2009). In this scheme, the tension is treated explicitly and the terms with highest-order derivatives in equation 2.25 are treated implicitly. Suppose we have evolved the membrane position until $n\Delta t$ and we need to march to $(n+1)\Delta t$. First, we compute the tension Σ_0 at the n th level using equation 2.29 as

$$\Sigma_0^n \sim \frac{(S^n - S^0)/\Delta t + \int_{-L/2}^{L/2} F h_{xxx} \left[\bar{K} h_{xxxx} - \frac{\beta}{2} (\varepsilon_r A^2 - C^2)_x \right] dx}{\bar{C} \int_{-L/2}^{L/2} F h_{xxx}^2 dx}, \quad (2.48)$$

where Δt is the time step, S^0 is the initial excess area and S^n is the excess area in equation 2.36 evaluated with h^n . The term $(S^n - S^0)/\Delta t$ in the numerator is the penalty term that adjusts the tension based on the deviation of membrane area from the initial value S^0 . A similar term has been used for an inextensible elastic filament (Tornberg & Shelley 2004). Second, the membrane position is updated via a semi-implicit time-step as

$$h^{n+1} + \Delta t \left[F^n (\bar{C} \Sigma_0^n h_{xx}^{n+1} - \bar{K} h_{xxxx}^{n+1})_x \right]_x = h^n - \Delta t \left[F^n \frac{\beta}{2} (\varepsilon_r (A^n)^2 - (C^n)^2) \right]_x, \quad (2.49)$$

where $F^n \equiv F(h^n)$. Third, the evolution equation for the electric field A (equation 2.28) is discretized as

$$\left(1 + \frac{g_m \Delta t}{c_m} \right) [(A^n - C^n) h^{n+1} - A^{n+1}] - \frac{\alpha}{c_m} A^{n+1} = \left(\frac{\Delta t}{c_m} - \frac{\alpha}{c_m} - 1 \right) A^n + (A^n - C^n) h^n - \Delta t \left(\nu' + \frac{g_m}{c_m} \nu \right). \quad (2.50)$$

$C^{n+1} = \sigma_r A^{n+1}$ for $\alpha = 0$, for $\alpha \neq 0$ we update the electric field C by solving the discretized evolution equation

$$C^{n+1} = \frac{\varepsilon_r \Delta t}{\alpha} \left[\left(1 - \frac{\alpha}{\Delta t} \right) A^n + \frac{\alpha}{\Delta t} A^{n+1} - \left(\frac{1}{\sigma_r} - \frac{\alpha}{\varepsilon_r \Delta t} \right) C^n \right]. \quad (2.51)$$

We solve for h^{n+1} , A^{n+1} and C^{n+1} simultaneously using the GMRES method.

For the periodic boundary conditions the spatial derivatives are computed using the spectral method (Canuto *et al.* 1986). Appropriate Δt and grid spacing Δx are chosen to keep the error in excess length S smaller than 0.1% of the initial excess length throughout the simulations. In the following we focus on periodic boundary conditions with $L = 2\pi$ unless otherwise specified.

The code is validated to be second-order in time and spectral in space. We numerically recover the analytical equilibrium profiles for a non-conducting membrane in a dc field. For a conducting membrane in a dc field, the same equilibrium profiles are numerically found for a given combination of (θ, S) while the equilibrium membrane tension Σ_0 now depends on the membrane conductance g_m as shown in figure 2(b). Figure 2(c) shows

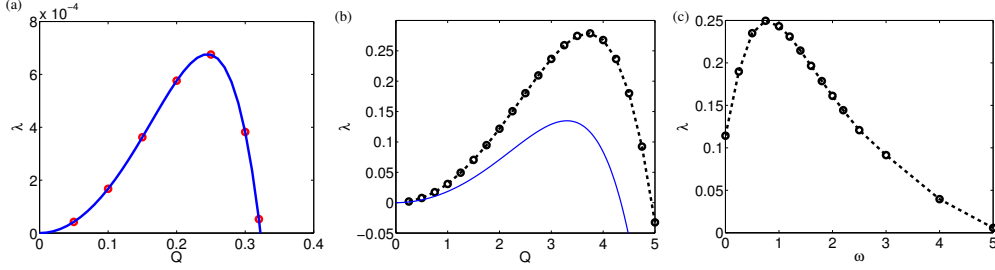


FIGURE 3. Linear growth rate for a tensionless flat membrane for $\beta = 1$. Solid curves are the linear growth rate λ for a dc field (equation 2.44), and symbols are from simulations. (a) Linear growth rate λ versus Q in a dc field with $(\varepsilon_r, \sigma_r, \mu_r, g_m, \bar{K}, \alpha) = (1, 10, 1, 1, 300, 0)$. (b) λ versus Q in an ac field with $\omega = 0.75$, $\nu = \sqrt{2} \sin(\omega t)$, $(\varepsilon_r, \sigma_r, \mu_r, g_m, \bar{K}, \alpha) = (1, 10, 1, 1.25, 10^{-2}, 0.1)$. (c) λ versus ω for $Q = 3.25$ and $(\varepsilon_r, \sigma_r, \mu_r, g_m, \bar{K}, \alpha) = (1, 10, 1, 1.25, 10^{-2}, 0.1)$.

the equilibrium profile for the electric field A_{eq} as the membrane conductance increases from bottom to top ($g_m \rightarrow \infty$ for the dash-dotted line).

3. Results

The linear instability of a flat planar membrane has been quantified (Seiwert & Vlahovska 2013) in terms of membrane conductance g_m , mismatch of fluid dielectric permittivity ε_r and conductivity σ_r , electric capillary number Ca and electric field frequency ω . In our long-wave formulation the time scale is based on the membrane charging time ($c_m = 1$), as a result their dimensionless (starred) parameters are related to ours as: $Ca^* = \frac{2\varepsilon_r \beta}{\bar{K}} \varepsilon$, $\xi^* = \frac{\bar{C}}{\bar{K}} \varepsilon^2$, and $\beta^* = \frac{\varepsilon_r \beta}{\mu_r} \varepsilon^{-3}$. In most electroformation experiments E_0 is often a few kV/m and h_0 is of the order of mm , with $\sigma_1 \sim 10^{-4} S/m$ and $\varepsilon = 0.3$ the range of β is computed as $1 \leq \beta \leq 2$. β can be as large as 600 for $h_0 \sim 10 mm$ and $E_0 \sim 30 kV/m$.

In § 3.1 we focus on the linear growth rate from numerical simulations for a tensionless flat membrane in both dc and ac fields. Based on the linear results we perform simulations to investigate the nonlinear dynamics of the membrane at different values of β in § 3.2 and excess length in § 3.3. In § 3.4 we demonstrate the alternating traveling wave on an inextensible membrane under an ac field. All the results are presented with $T = t/(2\pi/\omega)$, the time scaled to the period of the underlying ac field to help infer the underlying mechanisms.

3.1. Linear Stability of a Tensionless Flat Membrane in an ac Field

The membrane conductance destabilizes the planar membrane while the the linear growth rate is found to decrease with the frequency ω of the harmonic ac field from the Floquet analysis in (Seiwert & Vlahovska 2013). Here we first present numerical results to validate our code against the linear growth rate (equation 2.44) for a tensionless, flat membrane in dc electric field. We then present some numerical results to qualitatively compare with the Floquet results in figure 3 and figure 4 of Seiwert & Vlahovska (2013).

For the following calculations we use an initial membrane profile $h(x, 0) = 0.5 + 0.01 \cos(Qx)$ and 0 for both A and C . Figure 3(a) shows the linear growth rate under a dc field computed from the time evolution of the Fourier transform of h from simulations with $(\varepsilon_r, \sigma_r, \mu_r, g_m, \bar{K}, \alpha) = (1, 10, 1, 1, 300, 0)$. The solid curve is from equation 2.44 and the symbols are from numerical simulations of a tensionless flat membrane. Figure 3(b) shows the growth rate under an ac field with $\omega = 0.75$ and $\nu(t) = \sqrt{2} \sin(\omega t)$

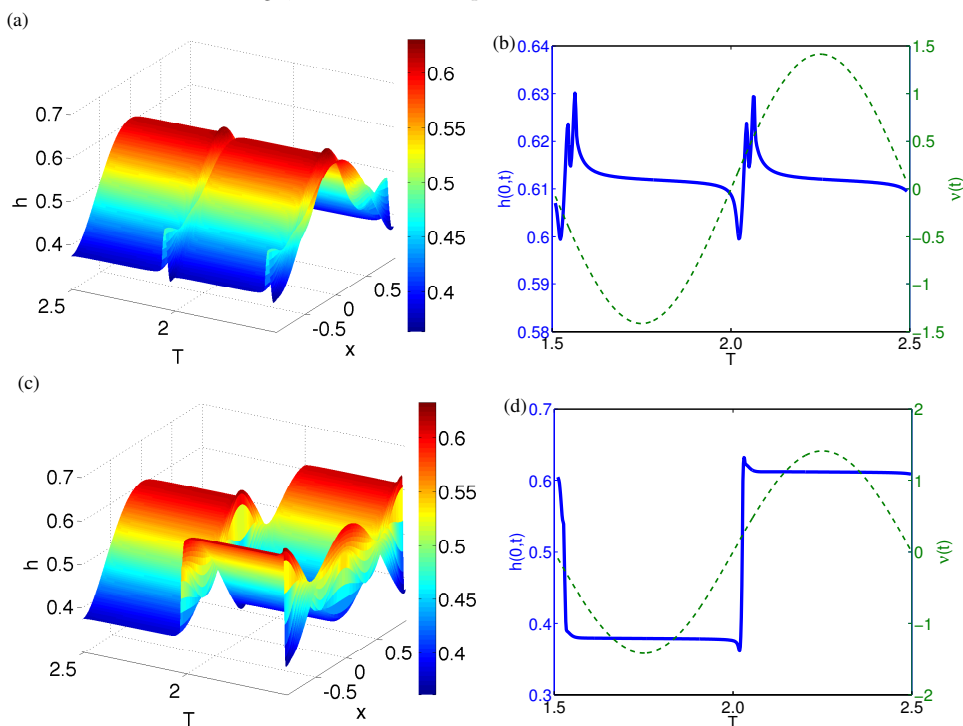


FIGURE 4. Membrane dynamics over one period for $\beta = 990$, $\omega = 0.75$, $\nu(t) = \sqrt{2}\sin(\omega t)$ (dashed line in panels (b) and (d)) and $(\varepsilon_r, \sigma_r, \mu_r, g_m, \bar{K}, \alpha) = (1, 10, 1, 1.25, 10^{-2}, 0.1)$. $\beta = 990$ for the top row, and $\beta = 6600$ for the bottom row. (a) and (c): Time-space plot of h . (b) and (d): The membrane height at $x = 0$ over one period.

for $(\varepsilon_r, \sigma_r, \mu_r, g_m, \bar{K}, \alpha) = (1, 10, 1, 1.25, 10^{-2}, 0.1)$. The solid curve is the dc growth rate from equation 2.44 with the same parameters. Figure 3(c) shows the dependence of the growth rate on the ac field frequency for $Q = 3.25$, $(\varepsilon_r, \sigma_r, \mu_r, g_m, \bar{K}, \alpha) = (1, 10, 1, 1.25, 10^{-2}, 0.1)$ and $\nu(t) = \sqrt{2}\sin(\omega t)$.

Our dimensionless frequency ω is the same as that in Seiwert & Vlahovska (2013) because we use the membrane charging time for the time unit. The electric potential for the base state is for an infinite domain in Seiwert & Vlahovska (2013), while for our analysis the base state electric potential is for a finite domain. As a result we focus on qualitative comparison here. The growth rate versus ω in figure 3(c) is in qualitative agreement with figure 3 of Seiwert & Vlahovska (2013): The linear growth rate decreases to zero as the frequency increases. The wave number dependence in figure 3(b) is also in qualitative agreement with results in figure 4 of Seiwert & Vlahovska (2013).

3.2. Effects of ac field magnitude β

In this subsection we fix $\omega = 0.75$ and $L = \pi/Q$ with $Q = 3.25$ where the linear growth rate λ is close to maximum for $(\varepsilon_r, \sigma_r, \mu_r, g_m, \bar{K}, \alpha) = (1, 10, 1, 1.25, 10^{-2}, 0.1)$ and $\nu(t) = \sqrt{2}\sin(\omega t)$ in figure 3(b) and (c). The excess length is fixed at $S = 0.1389$ as we increase β .

For small to moderate excess length S , the following dynamics is found as we vary the electric field strength β : For small β (top row in figure 4) the membrane profile stays close to the equilibrium profile under a dc field (determined by $S = 0.1389$ and $\theta = 0.5$) most of the time, except when the electric potential approaches zero and the membrane

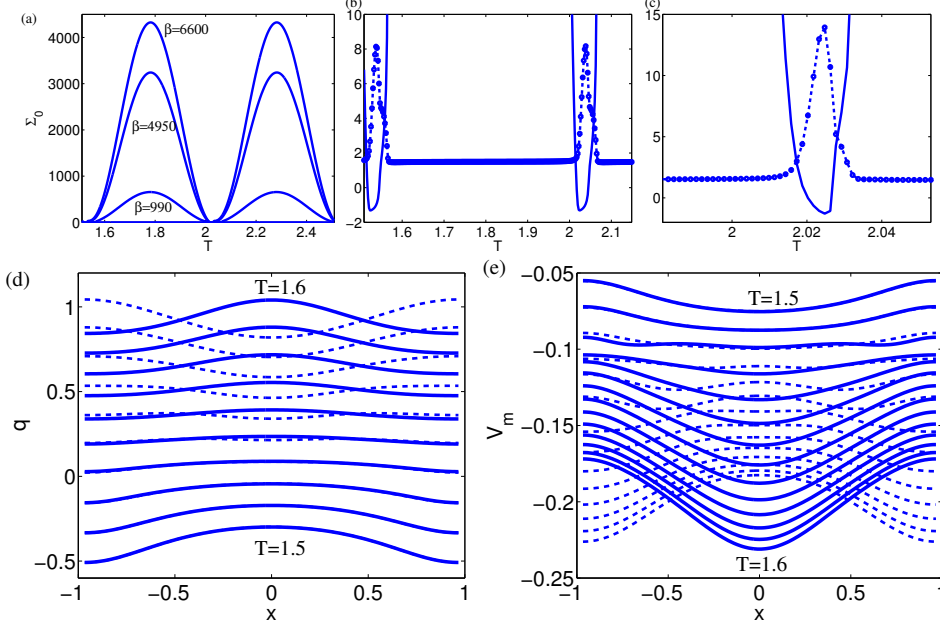


FIGURE 5. (a): Membrane tension Σ_0 over one period. From bottom to top, $\beta = 990$, 4950, and 6600. (b) Σ_0 (solid line) for $\beta = 990$ and $\langle \kappa^2 \rangle \equiv \int_{-L}^L \kappa^2 dx$ (dashed line). (c) Σ_0 (solid line) and $\langle \kappa^2 \rangle$ (dashed line) for $\beta = 6600$. Bottom row: Dynamics of the induced surface charge q (panel (d)) and transmembrane potential V_m (panel (e)) from $T = 1.5$ to $T = 1.6$ with $\Delta T = 0.1$ between two curves. Dashed curves are for $\beta = 990$ and solid curves are for $\beta = 6600$.

undergoes fast undulation as shown in figure 4. For large β (bottom row in figure 4) the fast membrane undulation leads to flip-flop of the membrane profile from h to $1 - h$. On the right panels (b) and (d) show the membrane height at $x = 0$ versus time (solid curves) with the dashed curves for the electric potential $\nu(t)$. For $\beta = 990$ we observe fast temporal oscillation around $\nu(t) \sim 0$, while for $\beta = 6600$ the membrane height overshoots as the profile flip-flops and then gradually reaches the equilibrium height.

The corresponding temporal variation of the membrane tension is shown in the top row of figure 5. Panel (a) shows Σ_0 for different values of β , and the correlation between Σ_0 and $\langle \kappa^2 \rangle = \int_{-L}^L \kappa^2 dx$ near the minimum of Σ_0 for $\beta = 990$ and $\beta = 6600$ are shown in panels (b) and (c), respectively. In panels (b) and (c) there are 10 time steps between two symbols with $\Delta t = 1/500$ for panel (b) and $\Delta t = 1/800$ for panel (c). Every half a period the membrane tension Σ_0 reaches a minimum, during when the membrane deformation amplifies. This is clearly illustrated by the concurrence of peaks in $\langle \kappa^2 \rangle$ (dashed lines in panels (b) and (c)) and the minimum in Σ_0 (solid lines in figure 5). The bottom row of figure 5 shows the variation in the surface induced charge density q and the transmembrane potential V_m . Depending on whether the membrane flip-flops or undulates (at high or low β) when Σ_0 is close to minimum, the distributions of q and V_m also vary with time differently: V_m (q) remains minimum (maximum) at $x = 0$ for the flip-flopping membrane, while the extrema of V_m (q) oscillate for the undulating membrane.

The above results show that the nonlinear dynamics of an inextensible elastic membrane in an ac field is closely related to the temporal variation of membrane tension Σ_0 , which is in sync with the external ac field $\nu(t)$ for small and moderate S . The membrane

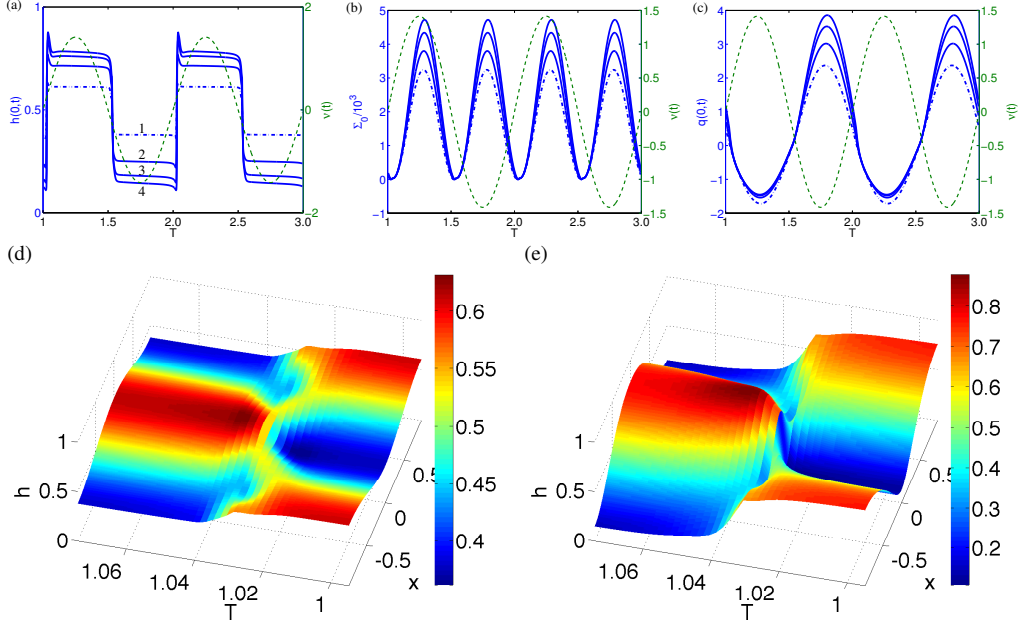


FIGURE 6. Flip-flopping dynamics of membrane with different excess length: $S = 0.139, 0.556, 0.868, 1.050$ for curves 1, 2, 3, and 4, respectively. $\beta = 4950$, $\omega = 0.75$, $\nu(t) = \sqrt{2}\sin(\omega t)$ and $(\varepsilon_r, \sigma_r, \mu_r, g_m, \bar{K}, \alpha) = (1, 10, 1, 1.25, 10^{-2}, 0.1)$. Top row: temporal variation of h , Σ_0 and q at $x = 0$. Bottom row: Flip-flopping of h for $S = 0.139$ (left) and $S = 1.050$ (right) when $\Sigma_0 \sim 0$.

deformation gets amplified when Σ_0 is around the minimum and $\nu(t)$ is around its mean. This may be understood by the linear instability of a tensionless membrane: When Σ_0 is close to zero the tensionless membrane is linearly unstable for $(\varepsilon_r - \sigma_r^2)(1 - \sigma_r)g_m > 0$. At large β the undulation of membrane is replaced by the flip-flop of membrane profile, and we observe overshoot in membrane height at $x = 0$ before and after the flip-flop. In addition we find higher surface charge density at $x = 0$ in figure 5(d), where the membrane height overshoots the most before and after the flip-flop (see figure 4).

At other times when Σ_0 are large, the membrane profile stays close to the analytic equilibrium membrane profile under a dc field. From simulations for higher membrane conductance we find that while membrane undulation still gets amplified when $\Sigma_0 \sim 0$, higher electric field is needed for the membrane flip-flop.

For $(\varepsilon_r, \sigma_r, \mu_r, g_m, \bar{K}, \alpha) = (1, 10, 1, 1.25, 10^{-2}, 0.1)$ the ac field strength has to be increased to very high values for different nonlinear membrane dynamics to kick in. However, based on the above results the nonlinear dynamics ensues only after the membrane turns linearly unstable when the membrane tension is almost zero. As the linear growth rate depends on β , σ_r and ε_r , it is reasonable to expect (and indeed we observe numerically) that the same nonlinear membrane dynamics can be found at smaller β , which is more physically realizable in the laboratory. For example, both the undulation and membrane flip-flop dynamics can be observed for β less than 200 when $(\varepsilon_r, \sigma_r, \mu_r, g_m, \bar{K}, \alpha) = (1, 50, 1, 0.01, 10^{-6}, 0.1)$.

3.3. Nonlinear dynamics at different excess length S

Here we investigate how membrane flip-flopping dynamics under a strong ac electric field may depend on the membrane excess length S . Figure 6(a) shows the variation of membrane height at $x = 0$ for four values of S (see caption). At $\beta = 4950$ we observe

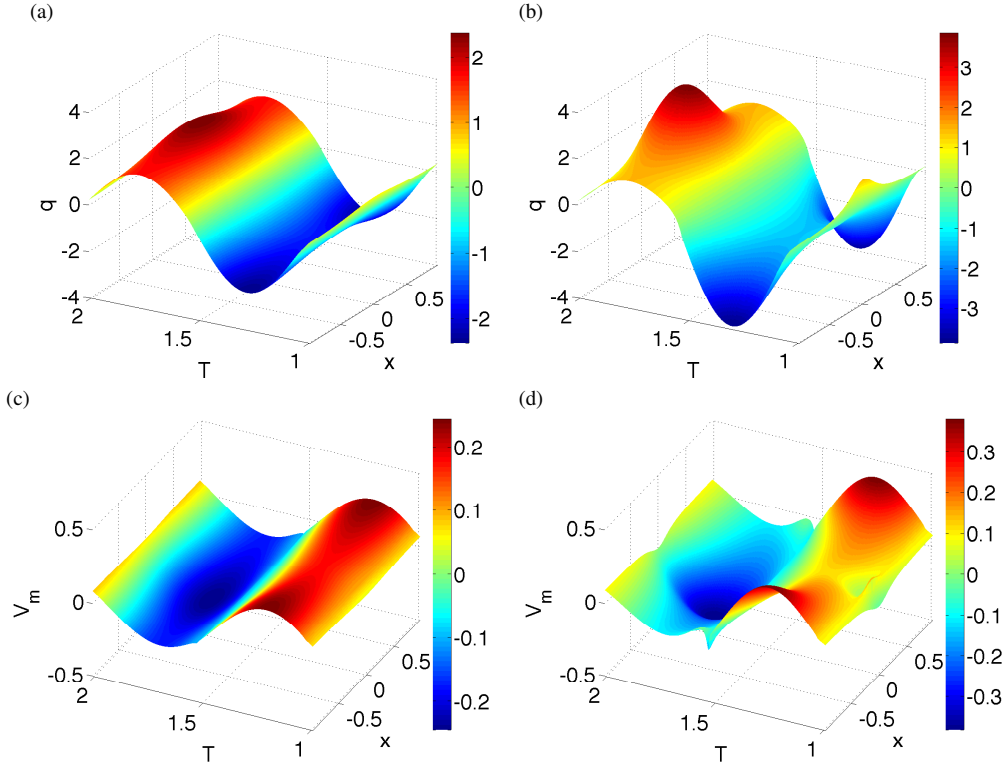


FIGURE 7. Variation of surface charge (top row) and transmembrane potential (bottom row) from the simulations in figure 6.

the overshoot in membrane height and the associated membrane flip-flopping for all four values of S . In addition we find that the overshoot in membrane height (when Σ_0 is close to zero, around its minimum) is enhanced as the excess length S increases from 0.1389 to 1.0501, as shown in figure 6(a). Figure 6(b) and (c) show the corresponding variation of Σ_0 and q at $x = 0$, where we see $\Sigma_0 \sim 0$ every half a cycle, corresponding to the overshoot in membrane height in figure 6(a). From (b) we note that the magnitude of Σ_0 increases with increasing S . Figure 6(d) and (e) show the space-time plots of the membrane profile when the membrane flip-flops.

We also observe that, even though the membrane flip-flops every half a cycle when $\Sigma_0 \sim 0$, the membrane height overshoots more when ν is positive. When ν is negative, Σ_0 reaches maximum and therefore stabilizes the membrane and suppresses the overshoot before and after the flip-flop. Such asymmetry between the $\nu > 0$ half cycle and the $\nu < 0$ half cycle is also reflected in the surface charge density: q dependence on S is amplified only when $\nu < 0$.

The corresponding space-time plots for q and V_m are shown in figure 7, where we observe the transmembrane potential is out of phase with q . As S increases, we observe the charge density to focus more at $x = 0$ around $T \sim 1.8$, right before the sudden overshoot in the membrane height and the fast change in at $T \sim 2$. In addition we observe the transmembrane potential at $x = 0$ has fast temporal variation when the membrane height flip-flops during the positive half cycles. During the negative half cycles, V_m has fast temporal variation at the end points.

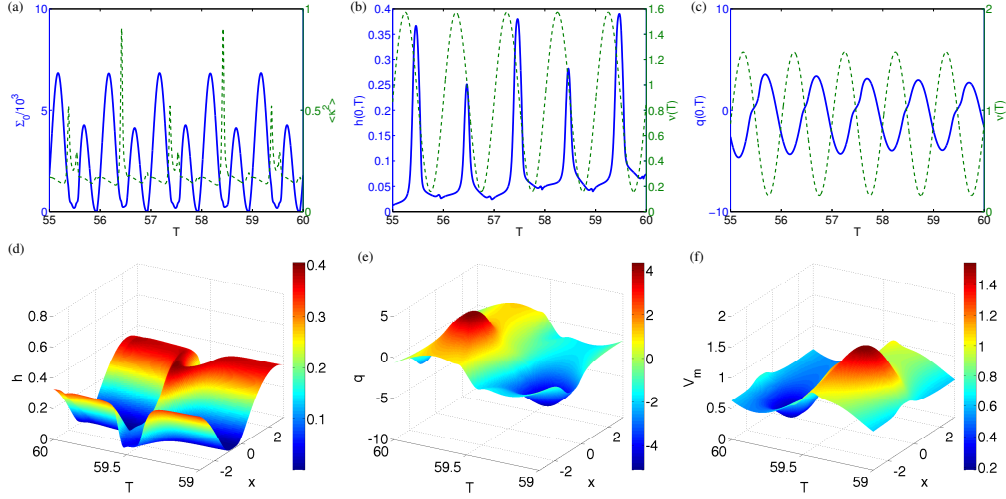


FIGURE 8. Non-periodic dynamics for $S = 0.1138$, $\theta = 0.2$, $\beta = 300$, $\omega = 0.05\pi$, $\nu(t) = \frac{\sqrt{3}}{2} + \frac{\sqrt{2}}{2} \sin(\omega t)$ and $(\varepsilon_r, \sigma_r, \mu_r, g_m, \bar{K}, \alpha) = (1, 60, 1, 0.01, 10^{-6}, 0.1)$. Top row: temporal variation of Σ_0 , h and q at $x = 0$. Bottom row: Time-space plots of membrane height, surface charge and transmembrane potential from $T = 59$ to $T = 60$.

3.4. Nonlinear “traveling” wave on an inextensible elastic membrane

For a given set of physical parameters $(\varepsilon_r, \sigma_r, \mu_r, g_m, \bar{K}, \alpha)$, the nonlinear membrane dynamics with sufficiently large electric field strength β and the membrane excess length S is no longer the periodic undulation or membrane flip-flop in § 3.2 and 3.3. Here we present an example from simulations for $S = 0.1138$, $\theta = 0.2$, $\beta = 300$, $(\varepsilon_r, \sigma_r, \mu_r, g_m, \bar{K}, \alpha) = (1, 60, 1, 0.01, 10^{-6}, 0.1)$, $\omega = 0.1\pi$ and $\nu(t) = \frac{\sqrt{3}}{2} + \frac{\sqrt{2}}{2} \sin(\omega t)$. 256 modes and $\Delta t = 1/100$ are used in the simulations.

Here the membrane is placed closer to the bottom electrode ($\theta = 0.2$), which is similar to the experimental setup for electroformation. At the beginning the membrane undergoes undulation when Σ_0 approaches minima. Very quickly the translational symmetry is broken and a direction for lateral movement (from right to left) is dictated by the initial condition, which is $h(x, 0) = 0.2 + 0.15 \cos(x) + 0.015(\cos(5x) + \sin(6x))$. The membrane moves oppositely from left to right as we invert the initial condition.

Figure 8(a) shows the temporal variation of Σ_0 (solid line) and $\langle \kappa^2 \rangle$ (dashed line), which illustrates the correlation between maxima in $\langle \kappa^2 \rangle$ and minima in Σ_0 . Figure 8(b) shows the membrane height at $x = 0$ (solid line) versus time for five periods, and the corresponding charge density is shown in panel (c). The dashed line in (b) and (c) is the electric potential $\nu(t)$. We see that Σ_0 reaches the minimum around the times when ν reaches its mean. While the tension Σ_0 remains positive within a cycle, a larger maximum is reached in the first half cycle than the second in (a). The variation of membrane height at $x = 0$ with T in (b) shows a maximum height is reached every half a cycle, with a clear indication of double-periodic dynamics. In (c) the surface charge density q at $x = 0$ oscillates with the same periodicity T with a slightly decreasing amplitude. Figure 8 (d), (e) and (f) show the time-space plots for h , q and V_m , respectively, over one period from $T = 59$ to $T = 60$.

Figure 9 shows the lateral membrane movement. In the top row we show the profiles of h , q and V_m at multiples of T from $T = 31$ (dashed curve) to $T = 42$ (solid curve). The inserts show a zoomed region from $T = 31$ (dashed curve) to $T = 34$. In (a) the insert

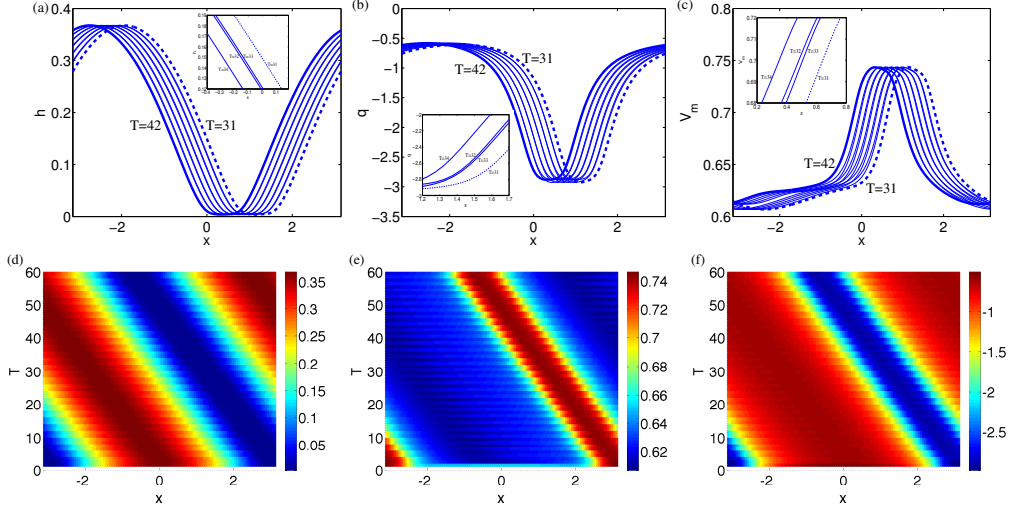


FIGURE 9. Temporal evolution at multiple periods of the ac field. Top row: Evolution of the membrane ((a)), surface charge ((b)) and transmembrane potential ((c)) from $T = 31$ to $T = 42$. Inserts show how Bottom row: Space-time plots of h in (a), q in (b), and V_m in (c).

shows that the membrane first makes a big step to the left from $T = 31$ to $T = 32$, then a small step to the right at $T = 33$ and then again a big step to the left at $T = 34$. Similar dynamics is found for q and V_m in (b) and (c), respectively. In the bottom row we show the time-space plots sampled at multiples of the periods. We clearly see a net movement from right to left in h in panel (d), q in panel (e) and V_m in panel (f). The membrane height can be quite close to the bottom electrode. Careful numerical convergence tests have been conducted to ensure that the nonlinear translational dynamics is not affected by h getting close to zero.

In deriving the long wave equation the horizontal velocity on the membrane is set to zero for local membrane inextensibility at the leading order. Consequently the alternating wave is actually a “coordinated” movement in the vertical direction like a Mexican wave in the soccer game: As the audience stand up and sit down in a rhythmic way, there appears to be a “traveling wave” moving in a directed fashion. The nonlinear dynamics conspires to coordinate such “dancing steps” for a traveling wave.

Increasing β further to $\beta = 600$, we find that the unidirectional traveling wave is replaced by a sloshing wave moving back and forth, almost in sync with the ac field. However it is not clear how physically realizable it is to have $\beta = 600$ in the microfluidic laboratory. We are now conducting thorough numerical investigation of the whole parameter space in $(\varepsilon_r, \sigma_r, \mu_r, g_m, \bar{K}, \alpha)$ to check if all these non-linear dynamics may be reproduced for physically reasonable electric field strengths.

4. Summary

In this work we investigate the long-wave nonlinear dynamics of an inextensible capacitive leaky (conducting) elastic membrane under electric fields. Using the sharp-interface approximation, the inextensible membrane behaves as a capacitive elastic sheet with a conductance due to ions leaking through the membrane. We derive a sixth-order nonlinear equation with an integral constraint from the membrane inextensibility in the long-wave limit. In a dc field where the displacement current is negligible, we analytically derive the equilibrium profile of a non-conducting membrane for a given excess length S and the

area θ under the planar membrane. We implemented a semi-implicit iterative scheme to numerically investigate the nonlinear dynamics of the membrane. Our long-wave model captures the linear behavior for a flat tensionless membrane, and we examine the different nonlinear dynamics under varying electric field strengths and excess length with physically relevant parameters in the simulations.

In our numerical simulations, both time step and grid spacing are adjusted to ensure (1) the error in the excess length is never exceeding 1% of the initial excess length throughout the simulations, and (2) numerically convergent solutions are obtained. Results in § 3.2 demonstrate the important role of membrane tension Σ_0 in membrane dynamics: Periodic undulation and flip-flopping of membrane are direct consequences of the linear instability of the membrane when the tension is close to zero. Results in § 3.3 show that the flip-flop of membrane profile gives rise to overshoot in membrane height when the external electric potential ν is increasing, and the magnitude of overshoot increases with the excess length S . During the membrane flip-flop we also find the surface charge density focusing at $x = 0$ where the membrane height overshoots. Such charge focusing at the highest-curvature location of the membrane is reminiscent of the Taylor cone formation in electrohydrodynamics (Fernandez de la Mora 2007).

Pillar formation at fixed locations is commonly observed for a fluid interface in an ac field (Roberts & Kumar 2009, 2010), where the fluid interface can be stretched indefinitely until the lubrication theory breaks down. At large excess length and under strong ac field, we find that after two cycles of membrane flip-flop the membrane height can get very close to the bottom wall, where $\min(h) \approx 10^{-3}$ for results in figure 8(d). The membrane then takes on an traveling motion from the double-periodic dynamics of the membrane movement of the sequence: a big step to the right, a small step to the left and then a big step to the right. Careful numerical convergence tests have been conducted to ensure that sufficient numerical resolutions are used to guarantee numerically convergent results and the traveling dynamics is not a numerical artifact. Within our long wave formulation we provide an explanation of the ‘‘Mexican Wave’’ for the ‘‘coordinated’’ traveling wave moving in $2 - 1$ steps. In our on-going research we include both (1) the Van der Waals force between the membrane and electrodes, and (2) the disjoining pressure to investigate the traveling wave and sloshing wave.

We are also extending the long-wave model in two directions: We are replacing the leaky dielectric fluids with electrolyte solutions where the bulk charges are not zero and the charges may accumulate away from the membrane. The membrane is found to be more linearly unstable in the presence of these charges near the membrane (Bazant *et al.* 2009). We are investigating how the membrane behave non-linearly in the electrolyte solutions. In addition we are also incorporating the membrane asymmetry due to the mismatch in lipid composition between the two leaflets. It will be interesting to examine how the asymmetry in the two leaflets might lead to different membrane dynamics and equilibrium shapes under external forces.

YNY acknowledges partial support from NSF grant DMS-1222550 and useful discussion with P. M. Vlahovska. SV acknowledges support from NSF grant DMS-1224656. MJM acknowledges support from NSF grant DMS-1312935. The simulations were conducted on the NJIT computing cluster, supported by NSF/MRI grant number DMS-0420590.

REFERENCES

- ANGELOVA, M. I. & DIMITROV, D. S. 1986 Liposome electroformation. *Faraday Discuss. Chem. Soc.* **81**, 303–311.
- ANTOV, Y., BARBUL, A., MANTSUR, H. & KORENSTEIN, R. 2005 Electroendocytosis: Exposure of cells to pulsed low electric fields enhances adsorption and uptake of macromolecules. *Biophysical Journal* **88**, 2206–2223.
- BAZANT, M. Z., KILIC, M. S., STOREY, B. D. & AJDARI, A. 2009 Towards an understanding of induced-charge electrokinetics at large applied voltages in concentrated solutions. *Adv. Coll. Int. Sci.* **152**, 48–88.
- BEZLYEPKINA, R., DIMOVA N., JORDO, M. D., KNORR, R. L., RISKE, K. A., STAYKOVA, M., VLAHOVSKA, P. M., YAMAMOTO, T., YANG, P. & LIPOWSKY, R. 2009 Vesicle in electric fields: some novel aspects of membrane behavior. *Soft Matt.* **5**, 3201–3212.
- BLOUNT, M. J., MIKSI, M. J. & DAVIS, S. H. 2012 Fluid flow beneath a semipermeable membrane during drying processes. *Phys. Rev. E* **85**, 016330.
- CANUTO, C., HUSSAINI, M. Y., QUARTERONI, A. & ZANG, T. A. 1986 *Spectral Methods in Fluid Dynamics*. New York: Springer-Verlag.
- CONSTANTIN, D., OLLINGER, C., VOGEL, M. & SALDITT, T. 2005 Electric field unbinding of solid-supported lipid multilayers. *Eur. Phys. J. E* **18**, 273–278.
- CRASTER, R. V. & MATAR, O. K. 2005 Electrically induced pattern formation in thin leaky dielectric films. *Phys. Fluids* **17** (3), 032104.
- FENG, J. Q. & BEARD, K. V. 1991 Three-dimensional oscillation characteristics of electrostatically deformed drops. *J. Fluid Mech.* **227**, 429–447.
- FERNANDEZ DE LA MORA, J. 2007 The fluid dynamics of Taylor cones. *Annu. Rev. Fluid Mech.* **39**, 217–243.
- HOSOI, A. E. & MAHADEVAN, L. 2004 Peeling, healing, and bursting in a lubricated elastic sheet. *Phys. Rev. Lett.* **93**, 137802.
- LACOSTE, D., LAGOMARSINO, M. C. & JOANNY, J. F. 2007 Fluctuations of a driven membrane in an electrolyte. *Europhys. Lett.* **77**, 18006.
- LACOSTE, D., MENON, G. I., BAZANT, M. Z. & JOANNY, J. F. 2009 Electrostatic and electrokinetic contributions to the elastic moduli of a driven membrane. *Eur. Phys. J. E* **28**, 243–264.
- LECUYER, S., FRAGNETO, G. & CHARITAT, T. 2006 Effect of an electric field on a floating lipid bilayer: A neutron reflectivity study. *Eur. Phys. J. E* **21**, 153–159.
- MCCONNELL, L. C., MIKSI, M. J. & VLAHOVSKA, P. M. 2013 Vesicle electrohydrodynamics in dc electric fields. *IMA Journal of Applied Mathematics* **78**, 797–817.
- ORON, A., DAVIS, S. H. & BANKOFF, S. G. 1997 Long-scale evolution of thin liquid films. *Rev. Mod. Phys.* **69**, 931–980.
- PEASE, L. F. & RUSSEL, W. B. 2002 Linear stability analysis of thin leaky dielectric films subjected to electric fields. *J. Non-Newtonian Fluid Mech.* **102**, 233–250.
- RISKE, K. A. & DIMOVA, R. 2005 Electro-deformation and poration of giant vesicles viewed with high temporal resolution. *Biophys. J* **88**, 1143–1155.
- ROBERTS, S. A. & KUMAR, S. 2009 Ac electrohydrodynamic instabilities in thin liquid films. *J. Fluid Mech.* **631**, 255–279.
- ROBERTS, S. A. & KUMAR, S. 2010 Electrohydrodynamic instabilities in thin liquid trilayer films. *Phys. Fluids* **22**, 122012.
- SADIK, M. M., LI, J., SHAN, J. W., SHREIBER, D. I. & LIN, H. 2011 Vesicle deformation and poration under strong dc electric fields. *Phys. Rev. E* **83**, 066316.
- SCHAFFER, E., THURN-ALBRECHT, T., RUSSELL, T. & STEINER, U. 2000 Electrically induced structure formation and pattern transfer. *Nature* **603**, 874–877.
- SCHWALBE, J. T., VLAHOVSKA, P. M. & MIKSI, M. 2011 Lipid membrane instability driven by capacitive charging. *Phys. Fluids* **23**, 04170.
- SEIFERT, U. 1995 The concept of effective tension for fluctuating vesicles. *Z. Physik. B* **97**, 299–309.
- SEIWERT, J., MIKSI, M. J. & VLAHOVSKA, P. M. 2012 Stability of biomimetic membranes in dc electric fields. *J. Fluid Mech.* **706**, 58–70.
- SEIWERT, J. & VLAHOVSKA, P. M. 2013 Instability of a fluctuating membrane driven by an ac electric field. *Phys. Rev. E* **87**, 022713.

- SENS, P. & ISAMBERT, H. 2002 Undulation instability of lipid membranes under an electric field. *Phys. Rev. Lett.* **88**, 128102.
- THAOKAR, R. M. & KUMARAN, V. 2005 Electrohydrodynamic instability of the interface between two fluids confined in a channel. *Phys. Fluids* **17**, 084104.
- TORNBERG, A.-K. & SHELLEY, M. J. 2004 Simulating the dynamics and interactions of flexible fibers in stokes flows. *J. Comp. Phys.* **196**, 8–40.
- VEERAPANENI, S. K., GUEFFIER, D., ZORIN, D. & BIROS, G. 2009 A boundary integral method for simulating the dynamics of inextensible vesicles suspended in a viscous fluid in 2d. *J. Comp. Phys.* **228** (7), 2334–2353.
- WEAVER, J. C. & CHIZMADZHEV, Y. A. 1996 Theory of electroporation: a review. *Bioelectrochem. Bioenerg.* **41**, 135–160.
- WU, N. & RUSSEL, W. B. 2009 Micro- and nano-patterns created via electrohydrodynamic instabilities. *Nanotoday* **4**, 180.
- ZHANG, J., ZAHN, J. D., TAN, W. & LIN, H. 2013 A transient solution for vesicle electrodeformation and relaxation. *Phys. Fluids* **submitted**.
- ZIEBERT, F., BAZANT, M. Z. & LACOSTE, D. 2010 Effective zero-thickness model for a conductive membrane driven by an electric field. *Phys. Rev. E* **81**, 031912.
- ZIEBERT, F. & LACOSTE, D. 2010 A poisson-boltzmann approach for a lipid membrane in an electric field. *New J. Phys.* **12**, 095002.
- ZIEBERT, F. & LACOSTE, D. 2011 A planar lipid bilayer in an electric field: membrane instability, flow field, and electrical impedance. *Advances in Planar Lipid Bilayers and Liposomes* **14**, 63–95.